Comparative Study of Inorganic Cluster−Surfactant Arrays

May Nyman,*,† David Ingersoll,† Seema Singh,‡ François Bonhomme,† Todd M. Alam,† C. Jeffrey Brinker,†,‡ and Mark A. Rodriguez†

Sandia National Laboratories, P.O. Box 5800, Albuquerque, New Mexico 87185, and University of New Mexico/NSF Center for Micro-Engineered Materials, Department of Chemical and Nuclear Engineering, Albuquerque, New Mexico 87131

Received February 12, 2005. Revised Manuscript Received April 9, 2005

We have investigated inorganic cluster−surfactant materials to better understand the structural evolution of these phases as the surfactant:cluster ratio increases above 4:1 and the cluster charge increases beyond −4. Our studies suggest that both ordering of the surfactant molecules into bilayers as well as the cluster charge are the primary influences on the hybrid cluster−surfactant phase structure. However, cluster geometry, inclusion of solvent molecules, surfactant tail length, cation head size, etc. also influence the self-assembly of these materials. We present the synthesis, characterization, and single-crystal X-ray structure of $[SiMo_{12}O_{40}][C_{16}H_{33}N(CH_3)_3]_4$ (monoclinic $P2_1/c$, $a = 13.136(1)$ Å, $b = 20.139(2)$ Å, $c = 41.030(3)$ Å, $\beta = 93.443(1)°$, and $V = 10834.7(17)$ Å^3) and the synthesis and characterization of a related phase that forms upon chemical reduction of the silicomolybdate anion. Structural and chemical comparisons are made between these two compounds, as well as other phases formed from polyoxometalates (with charges ranging from −3 to −16) and surfactants. The structure of $[SiMo_{12}O_{40}][C_{16}H_{33}N(CH_3)_3]_4$ is compared to the structures of other reported cluster−surfactant phases that also have a 1:4 cluster:surfactant ratio. Analyses of these phases provide some insight as to why it is thus far only this 1:4 ratio that provides crystals suitable for single-crystal diffraction studies and how the structure of the cluster−surfactant phases evolves as the surfactant/cluster ratio is increased.

Introduction

One strategy to self-assemble arrays of anionic metal−ligand (ligand = oxide, chalcogenide, halide, etc.) clusters is by organizing the clusters onto a cationic template such as a functionalized polycation[1,2] or an ordered array of surfactants[3,4] or other molecular cations.[1,5,6] These hybrid organic−inorganic materials have been synthesized predominantly by ion exchange/precipitation reactions,[7−9] layer-by-layer self-assembly,[1,10] and Langmuir−Blodgett or casting techniques.[3,11,12] For polyoxometalate (POM) anionic clusters, the resulting arrays feature surfaces or porous media that are highly accessible, ordered, and potentially exploitable for applications such as catalysis,[4,13] magnetism,[11] photoluminescence,[3] photochromism,[6] and proton conduction for fuel cells.[14] Additionally, the POM clusters that are charge-balanced by amphiphilic, monomeric cations are soluble in nonpolar solvents, which provide the opportunity to carry out further manipulations and investigations in nonaqueous media.[15−17] A further attraction of the cluster−surfactant hybrid phases is in their resemblance to biological material such as bilipid cell membranes, as well as their compatibility with biological molecules or organisms.[15−17]

A general structural model of ordered arrays composed of anionic POMs and cationic surfactants has been proposed from various characterization data including vibrational spectroscopies, powder X-ray diffraction or neutron diffraction, and UV−vis spectroscopy. Data from these studies suggest that the anionic clusters are either enclosed in hydrophobic shells or alternately layered with lipid bilayers. In particular, large clusters with high negative charges are described as surfactant-encapsulated clusters (SECs)[15−20] that

* To whom correspondence should be addressed. E-mail: mdnyman@sandia.gov.

† Sandia National Laboratories.

‡ University of New Mexico/NSF Center for Micro-Engineered Materials.

(1) Liu, S.; Volker, D.; Kurth, D. G. *J. Cluster Sci.* **2003**, *14*, 405.
(2) Feldheim, D. L.; Kim, H. M.; Hong, H. G.; Keller, S. W.; Grabar, K. C.; Natan, M. J.; Mallouk, T. E. Conference of the NATO Advanced Research Workshop on Modular Chemistry: Estes Park, CO, 1995; p 41.
(3) Wang, X. L.; Wang, Y. H.; Hu, C. W.; Wang, E. B. *Mater. Lett.* **2002**, *56*, 305.
(4) Tang, Z. Y.; Liu, S. Q.; Wang, E. K.; Dong, S. J.; Wang, E. B. *Langmuir* **2000**, *16*, 5806.
(5) Coronado, E.; Gomez-Garcia, C. J. *Chem. Rev.* **1998**, *98*, 273.
(6) Chen, Z.; Ma, Y.; Zhang, X.; Liu, B.; Yao, J. *J. Colloid Interface Sci.* **2001**, *240*, 487.
(7) Bonhomme, F.; Kanatzidis, M. G. *Chem. Mater.* **1998**, *10*, 1153.
(8) Rangan, K. K.; Kanatzidis, M. G. *Inorg. Chim. Acta* **2004**, *357*, 4036.
(9) Wachhold, M.; Kanatzidis, M. G. *Chem. Mater.* **2000**, *12*, 2914.
(10) Liu, S.; Kurth, D. G.; Bredenkotter, B.; Volkmer, D. *J. Am. Chem. Soc.* **2002**, *124*, 12279.
(11) Clemente-Leon, M.; Coronado, E.; Forment-Aliaga, A.; Romero, F. M. *C. R. Chimie* **2003**, *6*, 683.
(12) Clemente-Leon, M.; Coronado, E.; Delhaes, P.; Gomez-Garcia, C. J.; Mingotaud, C. *Adv. Mater.* **2001**, *13*, 574.
(13) Plault, L.; Hauseler, A.; Nlate, S.; Astruc, D.; Ruiz, J.; Gatard, S.; Neumann, R. *Angew. Chem., Int. Ed. Engl.* **2004**, *43*, 2924.
(14) Limoges, B. R.; Stanis, R. J.; Turner, J. A.; Herring, A. M. *Electrochim. Acta* **2005**, *50*, 1169.
(15) Kurth, D. G.; Lehmann, P.; Volkmer, D.; Colfen, H.; Koop, M. J.; Muller, A.; DuChesne, A. *Chem.—Eur. J.* **2000**, *6*, 385.
(16) Kurth, D. G.; Lehmann, P.; Volkmer, D.; Muller, A.; Schwahn, D. *J. Chem. Soc., Dalton Trans.* **2000**, 3989.
(17) Volkmer, D.; DuChesne, A.; Kurth, D. G.; Schnablegger, H.; Lehmann, P.; Koop, M. J.; Muller, A. *J. Am. Chem. Soc.* **2000**, *122*, 1995.
(18) Bu, W.; Wu, L.; Tang, A.-C. *J. Colloid Interface Sci.* **2004**, *269*, 472.
(19) Bu, W.; Li, W.; Li, H.; Wu, L.; Tang, A. C. *J. Colloid Interface Sci.* **2004**, *274*, 200.

10.1021/cm0503174 CCC: $30.25
Published on Web 00/00/0000 PAGE EST: 10.1

can be further organized in Langmuir−Blodgett type films.[16] Much of the evidence for the structure of the SECs is derived from small angle neutron and X-ray scattering, X-ray reflectance, and molecular modeling of the space requirements of surrounding a cluster with surfactant molecules.[15,16]

More rare and much more accurate structural descriptions have come from single crystal X-ray diffraction studies. These reveal the important features of cluster−surfactant organization including the tilt-angle of the surfactant tails, degree of surfactant interdigitation, inclusion of small solvent molecules, relative arrangement of the cluster and surfactant ions, and interactions of the oppositely charged species. This structural information is crucial for understanding chemical and physical behavior of the cluster−surfactant arrays. However, it remains challenging to grow well-ordered single crystals that diffract to high resolution to obtain a data set of sufficient quality for the determination and refinement of these large and low symmetry structures. To our knowledge, the cluster−surfactant phases that have been characterized by single-crystal X-ray diffraction include $[Ge_4E_{10}][C_nH_{2n+1}N(CH_3)_3]_4$ (E = S, Se; $n = 8-18$),[7,9] $[Ge_4S_{10}][CnH_{2n+1}NH_3]_4$ ($n = 12-18$),[8] $[Sn_2S_6][C_{12}H_{25}NH_3]_4 \cdot 2H_2O$,[21] $[Cr_2O_7][(C_{16}H_{33})_2N(CH_3)_2]_2$,[22] $[H_2V_{10}O_{28}][C_{12}H_{25}N(CH_3)_3]_4$,[23,24] and $[Mo_6O_{19}][(C_{18}H_{36})_2N(CH_3)_2]_2$.[25] These phases are all lamellar, composed of alternating lipid bilayers and layers of anionic clusters.

Other cluster−surfactant phases that have been described as approximately lamellar from powder X-ray diffraction data and TEM data include $[Nb_xW_{6-x}O_{19}]^{(2+x)-}[(C_{16}H_{33})_2N(CH_3)_2]_{2+x}$ ($x = 2, 3, 4$),[26] $[PW_{11}O_{39}][C_{12}H_{25}N(CH_3)_3]_7$,[27] $[H_2W_{12}O_{40}][C_{12}H_{25}N(CH_3)_3]_6$,[23,26] and phases featuring vanadium borophosphate cluster anions.[28] The striking observation noted from this literature review is that in every case in which a single-crystal structure was obtained for these cluster−surfactant materials, the ratio of the cluster to surfactant tail is 1:4. Either a −4 cluster is charge-balanced by four surfactant molecules with single tails or a −2 cluster is paired with two double-tail surfactant molecules. Since it seems it is only this 1:4 ratio that gives high quality single-crystals of the cluster−surfactant phases, we postulate that this ratio provides optimum space-filling and ion packing to form well-ordered layers of anionic clusters and lipid bilayers. At the other structural extreme where the cluster charge is around −20 to −40, the surfactant layer encloses the cluster in a spherical fashion, as is described for the SEC phases. However, there is a paucity of detailed structural data or molecular models that describe these cluster−surfactant arrays for clusters with charges in the intermediate range between approximately −5 to −20. It is likely that with these intermediate surfactant/cluster ratios the arrangement of the anionic cluster and the arrangement of the correct number of charge-balancing amphiphilic cations is not well-matched and that the lipid bilayers and anionic cluster layers cannot form a highly ordered material. In fact, the structure resulting from relative arrangement of anionic clusters with an approximately −5 to −20 charge and lipid bilayers is likely to be intermediate between alternating flat layers and enclosed spheres. In the very thorough study of POM−surfactant phases by Stein et al.,[26] the layers of $[H_2W_{12}O_{40}][C_{12}H_{25}N(CH_3)_3]_6$ are described as undulated, as they are observed by TEM. Furthermore, for the niobo-tungstate Lindquist ion phases, the cluster surfactant phase featuring a −4 cluster is described as better crystallized than the related phases featuring the −5 and −6 clusters.[26]

Structural information regarding the evolution of these cluster−amphiphile phases from ordered layers to surfactant-encapsulated clusters would be extremely valuable in relating structure−property characteristics of functional coatings or films that contain clusters of intermediate charge (i.e., −5 to −20).[29] Additionally, such information could be utilized for crystal engineering, in providing insight into how these phases might be better ordered so that single-crystal structures may be obtained.

In this investigation, we present a single-crystal X-ray diffraction study of $[SiMo_{12}O_{40}][C_{16}H_{33}N(CH_3)_3]_4$, a cluster-surfactant phase with a 1:4 cluster/surfactant ratio. Its synthesis and structural characterization are described, and the structure is discussed in terms of understanding and rationalizing the ideal 1:4 ratio for forming undistorted layers. In addition, the silicomolybdate−surfactant phase was reduced, and this reduction product is compared to the 1:4 phase to gain some understanding of the structural evolution of a cluster−surfactant array as it is chemically altered. Finally, a variety of these C_{16}−surfactant salts of polyoxometalates with a cluster charge ranging from −3 to −16 were synthesized and characterized by transmission electron microscopy (TEM) and X-ray powder diffraction. All attempts to grow good quality single crystals of these phases were unsuccessful, confirming our initial thoughts that it is not easily accomplished.

Experimental Procedures

General Laboratory and Instrumentation. Silicomolybdic acid, phosphotungstic acid, cetyltrimethylammonium bromide (CTABr), and solvents (acetonitrile, methylethyl ketone, miscellaneous alcohols) were all purchased from Aldrich and used as received. The polyoxoniobate salts, $Na_7[HNb_6O_{19}] \cdot 14H_2O$,[30] $Na_8[Ti_2Nb_8O_{28}] \cdot 34H_2O$,[31] $Na_{14}[H_2Si_4Nb_{16}O_{56}] \cdot 45.5H_2O$,[32] and $Na_{16}[SiNb_{12}O_{40}] \cdot 4H_2O$[33] were synthesized as previously reported. X-ray

(20) Bu, W.; Wu, L.; Hou, X.; Fan, H.; Hu, C.; Zhang, X. *J. Colloid Interface Sci.* **2002**, *251*, 120.
(21) Li, J.; Marler, B.; Kessler, H.; Soulard, M.; Kallus, S. *Inorg. Chem.* **1997**, *36*, 44697.
(22) Fosse, N.; Brohan, L. *J. Solid State Chem.* **1999**, *145*, 655.
(23) Janauer, G. G.; Dobley, A. D.; Guo, J.; Zavalij, P. Y.; Whittingham, M. S. *Chem. Mater.* **1996**, *8*, 2096.
(24) Janauer, G. G.; Dobley, A. D.; Zavalij, P. Y.; Whittingham, M. S. *Chem. Mater.* **1997**, *9*, 647.
(25) Ito, T.; Sawada, K.; Yamase, T. *Chem. Lett.* **2003**, *32*, 938.
(26) Stein, A.; Fendorf, M.; Jarvie, T. P.; Mueller, K. T.; Benesi, A. J.; Mallouk, T. E. *Chem. Mater.* **1995**, *7*, 304.
(27) Taguchi, A.; Abe, T.; Iwamoto, M. *Micropor. Mesopor. Mater.* **1998**, *21*, 387.
(28) Do, J.; Jacobson, A. J. *Chem. Mater.* **2001**, *13*, 2436.
(29) Clemente-Leon, M.; Agricole, B.; Mingotaud, C.; Gomez-Garcia, C. M.; Coronado, E.; Delhaes, P. *Langmuir* **1997**, *13*, 2340.
(30) Alam, T. M.; Nyman, M.; Cherry, B. R.; Segall, J. M.; Lybarger, L. E. *J. Am. Chem. Soc.* **2004**, *126*, 5610.
(31) Nyman, M.; Criscenti, L. J.; Bonhomme, F.; Rodriguez, M. A.; Cygan, R. T. *J. Solid State Chem.* **2003**, *176*, 111.
(32) Nyman, M.; Bonhomme, F.; Alam, T. M.; Rodriguez, M. A.; Cherry, B. R.; Krumhansl, J. L.; Nenoff, T. M.; Sattler, A. M. *Science* **2002**, *297*, 996.

powder diffraction was performed with a Bruker D8 Advance Diffractometer in Bragg−Brentano geometry with Ni-filtered CuKα radiation. All POM−surfactant phases were deposited from solution on a mica (001) face, so that the d001 = 9.98 Å mica peak could be used for calibrating the basal plane peak positions. The $[SiMo_{12}O_{40}][CTA]_4$ phase (CTA = cetyltrimethylammonium) and the related reduced phase were deposited from acetonitrile solution, $[PW_{12}O_{40}][CTA]_3$ from an acetone solution, $[HNb_6O_{19}][CTA]_7$ and $[Ti_2Nb_8O_{28}][CTA]_8$ from ethanol solutions, and $[H_2Si_4Nb_{16}O_{56}]$-$[CTA]_{14}$ and $[SiNb_{12}O_{40}][CTA]_{16}$ from butanol solutions. Infrared spectra (370−4000 cm^{-1}) were recorded on a Perkin-Elmer Spectrum GX FTIR using the KBr pellet method. Samples were examined with a JEOL JSM-6300V scanning electron microscope equipped with a Link GEM Oxford detector and IRIDIUM IXRF Systems software for EDAX analysis. TEM experiments were performed with a JEOL 2010 microscope. Since the organic portion of these materials was sensitive to decay under the electron beam, a Gatan smartset model 900 cold stage was used for enhanced imaging. All the images were taken at −180 °C. Samples for TEM analysis were mounted as a dry powder onto the carbon grid filled with holes. Compositional analysis of the silicomolybdate phases was done by Galbraith Laboratories, Knoxville, TN.

All electrochemical data were collected using a BAS100B potentiostat in a three-electrode cell. The working electrode was a freshly polished glassy carbon electrode having a diameter of 3 mm, and a Pt coil was used as the counter electrode. A Ag/AgCl saturated KCl reference electrode was used throughout, and unless otherwise noted, all potentials are referenced to it. All solutions were deoxygenated by bubbling with Ar prior to making any measurements or sample preparations and were blanketed with Ar while the measurements were being made. The supporting electrolyte solution was comprised of a 90:10 mixture of acetonitrile and an aqueous solution of 1 M H_2SO_4 providing a final concentration of 0.1 M H_2SO_4. Solutions of the CTA silicomolybdates were prepared by dissolution of the compound in the deoxygenated supporting electrolyte solution. Concentrations were typically in the range of 2 mg mL^{-1}.

Synthesis of $[SiMo_{12}][CTA]_4$. $[SiMo_{12}O_{40}][C_{16}H_{33}N(CH_3)_3]_4$, $[SiMo_{12}][CTA]_4$ for short, was synthesized simply by combining aqueous solutions of silicomolybdic acid ($H_4SiMo_{12}O_{40}$, FW = 1824) and cetyltrimethylammonium bromide (CTABr, $C_{16}H_{33}N(CH_3)_3Br$, FW = 364) in a 1:4 ratio (for example, 0.5 g of silicomolybdic acid and 0.4 g of CTABr; each dissolved in ∼20 mL of DI water). The pH of the silicomolybdate solution was around 2, and the pH of the CTABr phase was 6−7. A yellow flocculate immediately formed upon combining the two clear solutions. The flocculate was collected in a Buchner funnel by vacuum filtration and rinsed several times with water to rid it of eliminated HBr and any excess CTABr. Lamellar single crystals of $[SiMo_{12}][CTA]_4$, up to 5 × 5 mm, were obtained by dissolution in hot acetonitrile and recrystallization upon standing at room temperature. Weight % experimental (calculated): Mo, 39.01 (38.97); Si, 1.10 (0.95); C, 30.91 (30.85); N, 1.93 (1.89); and H, 5.74 (5.68).

Reduced $[SiMo_{12}]$-[CTA] was obtained generally by heating $[SiMo_{12}][CTA]_4$ at 140 °C in a 23 mL Parr pressure reactor containing a mixture of water and 2-butanone (methyl ethyl ketone, MEK). Some variations in experimental parameters were made including: (1) a reduction process carried out with and without the addition of excess CTABr, (2) ratio of water to MEK (ranging from 1:9 to 1:1), and (3) heating time (3−7 days). The only parameter that significantly affected the final product was the heating time. The phase that was used for all characterizations described in the following sections was produced by combining $[SiMo_{12}][CTA]_4$ (0.5 g, 0.17 mmol) plus CTABr (0.10 g, 0.34 mmol) in a 1:1 mixture of MEK and water (4 mL of H_2O, 4 mL of MEK) and heating it in a 23 mL Parr pressure at 140 °C for 3 days. For all experiments, a deep green to deep blue precipitate was obtained that was collected by vacuum filtration. Weight % experimental: Mo, 39.93; Si, 1.19; C, 28.23; N, 1.72; and H, 5.23.

Table 1. Crystallographic Information for $[SiMo_{12}][CTA]_4$

chemical formula	$C_{76}H_{168}N_4O_{40}SiMo_{12}$
formula weight	2957.5
T (K)	203 (2)
wavelength (Å)	0.71069
crystal system	monoclinic
space group	$P2_1/c$
a (Å)	13.136 (1)
b (Å)	20.139 (2)
c (Å)	41.030 (3)
β (deg)	93.443 (1)
volume (Å^3)	10834.7(17)
Z	4
D_{calc} (g/cm^3)	1.813
absorption coefficient (mm^{-1})	1.43
F(000)	5960
crystal size (mm)	0.25 × 0.18 × 0.13
2θ max (deg)	50.46
index ranges	$-15 \le h \le 15$, $-23 \le k \le 24$, $-49 \le l \le 49$
reflections collected	79462
independent reflections	19494; 14906 with Fo > $4\sigma(F_o)$
Rint	0.0587
refinement method	full-matrix least-squares on F^2
data/parameters	19494/1198
goodness-of-fit on F^2	1.081
final R indices [F_o > 4_(F_o)]	$R_1 = 0.0479$, $wR_2 = 0.0896$
R indices (all data)	$R_1 = 0.0714$, $wR_2 = 0.0983$
largest diff. peak and hole	1.72 /−1.42 e Å^{-3}

Synthesis of Additional POM-CTA Phases. Phases synthesized include $[PW_{12}O_{40}][CTA]_3$, $[HNb_6O_{19}][CTA]_7$, $[Ti_2Nb_8O_{28}][CTA]_8$, $[H_2Si_4Nb_{16}O_{56}][CTA]_{14}$, and $[SiNb_{12}O_{40}][CTA]_{16}$. For each surfactant salt, the sodium salt (polyoxoniobates) or acid (phosphotungstate) of the polyoxometalate was dissolved in deionized water in quantities ranging from 0.1 to 2.0 g. The stoichiometric equivalent (equivalent to the charge of the cluster) of CTABr was dissolved in a second vial of deionized water, usually with heating. The surfactant solution was then added to the polyoxometalate solution, and a white flocculant was immediately precipitated in every case. This powder was collected by filtration and washing with water to ensure removal of all eliminated NaBr or HBr.

X-ray Data Collection for $[SiMo_{12}][CTA]_4$. Single-crystal diffraction: a parallelepipedic crystal of **1** was mounted with fluorolube on a glass fiber and transferred in the cold nitrogen stream of a Bruker SMART CCD diffractometer. Data were collected at 203 K using graphite monochromatized MoKα radiation and were processed with SAINT. The structure was solved by direct methods (program SIR97) and refined by full matrix least-squares (program SHELXL97). All non-hydrogen atoms were refined anisotropically. Hydrogen atoms were placed geometrically and refined isotropically using the riding-atom model. The refinement of the 1198 parameters eventually converged to $R_1 = 4.79\%$ for 14 906 reflections with $F_o > 4\sigma(F_o)$ and $R_1 = 7.14\%$ for all 19494 data. Relevant parameters for the data collection and refinement are given in Table 1.

Results

Synthesis of Silicomolybdate−CTA Phases. The synthesis and recrystallization of $[SiMo_{12}][CTA]_4$ was straightforward. Further details regarding its chemical behavior and

(33) Nyman, M.; Bonhomme, F.; Alam, T. M.; Parise, J. B.; Vaughan, G. M. B. *Angew. Chem., Int. Ed. Engl.* **2004**, 2787.

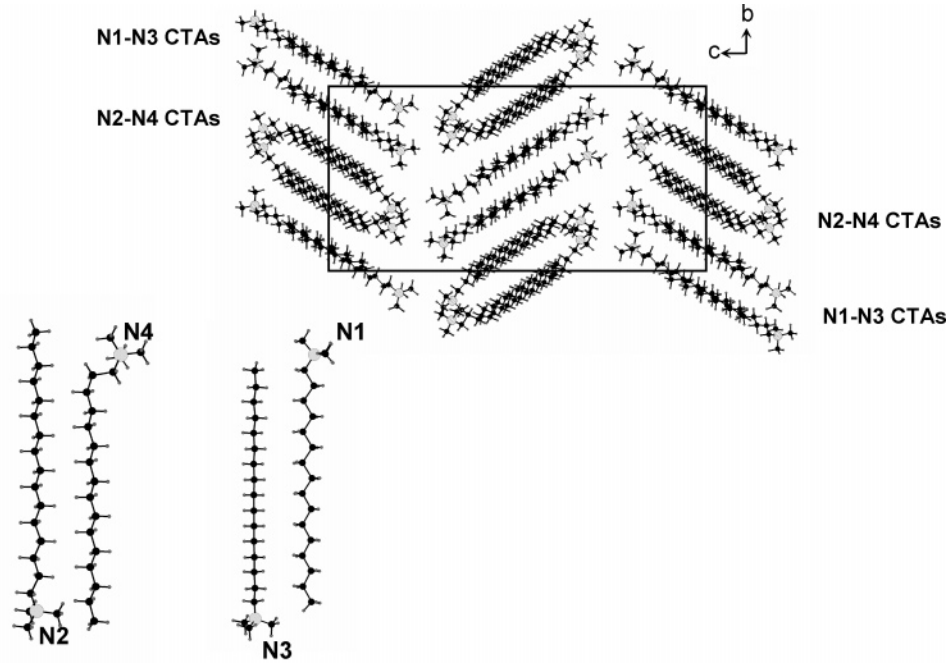

Figure 1. Top: view along the *a*-direction of the lipid bilayers of interdigitated CTA cations of $[SiMo_{12}][CTA]_4$ emphasizing the alternating pairs of rows of interdigitated CTA N1−N3 and N2−N4 cations where N1, N2, N3, and N4 denote the N-atom of the trimethylammonium head. Bottom: view of interdigitated N1−N3 CTA cations and N2−N4 CTA cations.

characterization are described in the following sections. In the formation of the reduced phase, for some experiments, we used a 2:1 ratio of CTABr:$[SiMo_{12}][CTA]_4$ to provide excess CTA cations for charge-balancing the reduced cluster. However, reduction of the silicomolybdate cluster takes place with or without CTABr, which suggests that bromide does not partake in the reduction event. SEM-EDS analysis of the reduced silicomolybdate−CTA phases confirmed that there was no bromine contamination in these samples. Oxidation of 2-butanone is a well-known reaction, so it is this solvent that is most likely responsible for the reduction of silicomolybdate. One paper described the oxidation of 2-butanone by dodecatungstocoboltate (III) in the presence of water to form acetaldehyde and acetic acid as major oxidation products.[34] This reaction is proposed to take place by a free radical mechanism, and protons are released (which is likely why we observed protons in the reduced phase). Qualitatively, we know a fraction of the silicomolybdate clusters is reduced by the MEK/water treatment, as evidenced by the color of the powder product that ranges from deep green to deep blue. Longer treatment (up to 7 days) of $[SiMo_{12}][CTA]_4$ resulted in reduction of more clusters. For the majority of our characterization studies, we utilized the 3-day reduction product.

Structural Description of $[SiMo_{12}][CTA]_4$. Along the *c*-direction, layers of the $[SiMo_{12}O_{40}]^{4-}$ Keggin ions alternate with bilayers of interdigitated CTA cations. The trimethylammonium heads of the CTA cations penetrate the layers of negatively charged Keggin ions, and the lipid tails interdigitate with the tails of a second layer of CTA cations, whose ammonium heads point in the opposite direction. The surfactant chains are not oriented normal to the plane of the Keggin ions. Rather, the angle between the C_{16} chains and the inorganic, anionic layers is around 35°, which is typical of interdigitated single-chain surfactants.[35] In Figure 1, a view down the *a*-axis shows the layers of interdigitated chains only. Alternating lipid bilayers do not tilt in the same direction; therefore, there are two lipid bilayers in the unit cell. There are four independent CTA cations, denoted by their ammonium nitrogen atoms in this discussion as N1, N2, N3, and N4. The N1 and N3 CTA cations interdigitate in pairs of rows, and the rows are aligned down the *a*-axis (see Figure 1). Likewise, the N2 and N4 CTA cations interdigitate in pairs of rows that are also aligned along the *a*-axis. The pairs of rows alternate between N1−N3 and N2−N4 along the *b*-direction. Figure 1 shows the relative position between the N1 and the N3 cations and between the N2 and N4 cations. The N1, N2, and N3 CTA cations are all straight, whereas the N4 cation is bent between the second and the third carbon from the nitrogen (see Figure 1). All of the CTA chains can be described as interdigitated by a length of 14 carbons, and the first two carbons from the ammonium head are not interdigitated. The approximate distance between chains in the interdigitated region is 2.6−3.2 Å, as measured by the closest H−H distance between two neighboring chains.

The Keggin ions are ordered within their layers as a two-dimensional hexagonal array; each Keggin ion is surrounded by six other Keggin ions (Figure 2a). The tetramethylammonium heads penetrate the anionic layers significantly on both sides of the layer, as is illustrated in Figure 2b. This can be seen by the N−N distances across a Keggin ion layer: the N2−N3 distance is around 5.8 Å, and the N1−N4 distance is around 5.9 Å. The Keggin ions can be described as a sphere that is 10.3 Å in diameter. Thus, the

(34) Gupta, M.; Saha, S. K.; Banerjee, P. *Intl. J. Chem. Kinetics* **1990**, *22*, 81.

(35) Kunitake, T. *Angew. Chem., Int. Ed. Engl.* **1992**, *31*, 709.

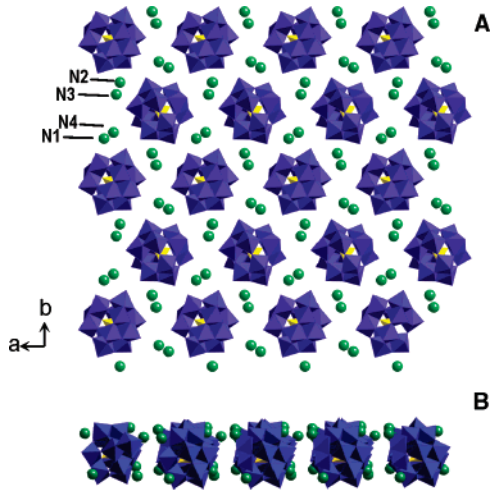

Figure 2. View down the *c*-axis of $[SiMo_{12}][CTA]_4$ showing the Keggin ion (blue) layers and the nitrogen atoms (green) of the trimethylammonium heads of the CTA cations located on both sides of the inorganic layer **(**A**)** and view of these same species, as seen parallel to the Keggin ion layers (B).

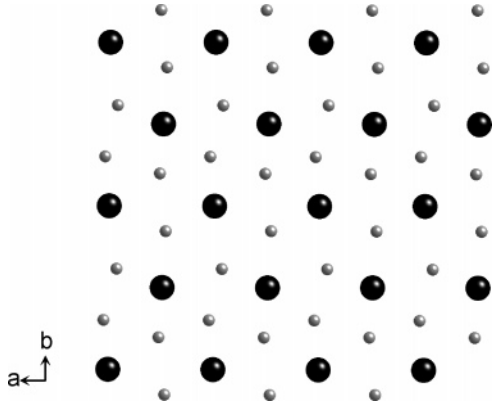

Figure 3. Simplified representation of the charged species of $[SiMo_{12}][CTA]_4$, viewed down the *c*-axis. The black spheres represent the silicomolybdate Keggin ions, and the gray spheres are the nitrogen atoms of a single layer of trimethylammonium heads of the CTA cations.

Keggin layers and ammonium head layers are interpenetrating by ∼2.2 Å on each side of the inorganic layer.

All bond angles and bond distances of the $[SiMo_{12}O_{40}]^{4-}$ anions and CTA cations are within normal range and do not warrant further discussion. Both the tetramethylammonium heads and the Keggin ions are arranged in the *ab*-plane in hexagonal arrays, where the packing of the Keggin clusters is more regular and the packing of the surfactant cations is more distorted. This is best illustrated in Figure 3, where both the trimethylammoniums and the Keggin ions are represented by spheres. The hydrogens of the ammonium methyls are not strongly H-bonded to the Keggin ion oxygens, in that the closest H(methyl)−O(Keggin) distance is around 2.6 Å. Each trimethylammonium is located between three Keggin ions, and every Keggin ion is sandwiched between two hexagonal crowns of trimethylammonium headgroups. In this arrangement, every Keggin ion is associated with 12 trimethylammoniums, each of which is shared between three Keggin ions, which accounts for the 1:4 ratio of $[SiMo_{12}O_{40}]^{4-}$ to CTA.

Comparison of $[SiMo_{12}][CTA]_4$ and Reduced $[SiMo_{12}]$−CTA. $[SiMo_{12}][CTA]_4$ (also referred to here as the 1:4 phase) has the typical yellow color of a silicomolybdic acid that is fully oxidized. Likewise, the reduced $[SiMo_{12}]$ −CTA phase has the greenish-blue hue of a compound containing reduced silicomolybdate anions.[36] Both the 1:4 and the reduced $[SiMo_{12}]$ compounds are soluble in acetonitrile. However, the 1:4 compound requires heating for dissolution and quickly recrystallizes upon cooling. The reduced $[SiMo_{12}]$ −CTA compound, on the other hand, quickly dissolves at room temperature at high concentrations and is more reluctant to reprecipitate. The difference in solubility characteristics is likely a result of the relative stability of the 1:4 solid phase due to its high degree of cation−anion ordering and deep interdigitation of the surfactant tails (see following discussion).

The compositional analysis of the 1:4 phase agreed very well with the calculated composition (as determined from the X-ray diffraction structure). On the other hand, we were initially surprised by the compositional analysis of the reduced $[SiMo_{12}]$−CTA phase. Since the average silicomolybdate anion charge of the blue phase was expected to be greater than that of the yellow phase, we likewise expected more surfactant molecules present in the blue phase for charge-balancing. However, the concentration of Mo, Si, C, N, and H in the blue phase is close to that of the 1:4 phase. In fact, the concentrations suggest that the reduced phase has a little less than four CTA molecules per cluster. On the basis of weight % Mo, the element that gave the most accurate chemical analysis for the 1:4 phase, the ratio of the cluster to CTA of the reduced phase is around 1:3.75. Infrared spectroscopy of the 1:4 phase and the reduced phase shed some light on these unexpected results. Vibrational bands at 3543, 3373, 1690, and 1600 cm^{-1} are observed in the reduced phase but not in the 1:4 phase. The sharper adsorption at 3543 cm^{-1} is likely to be a proton sited on the water molecule as an H_3O^+.[37] The broader bands at 3373, 1690, and 1600 wavenumbers can be attributed to H_2O. The presence of protons in the reduced phase would account for the 1:3.75, $[SiMo_{12}O_{40}]$:CTA, ratio, in that fewer CTA molecules are required to charge-balance the $[SiMo_{12}O_{40}]$ anions if charge-balancing protons are present as well. The protons were likely produced as a byproduct of 2-butanone oxidation, as stated previously.

^{29}Si MAS NMR of the silicomolybdate phases was also used to compare the anionic species of these silicomolybdate compounds. The 1:4 phase gave a single sharp peak at −74.9 ppm (fwhm = 60 Hz) corresponding with Si in a very symmetric tetrahedral environment. The reduced phase has two ^{29}Si peaks: that of the 1:4 phase at −74.9 ppm and a second one significantly shifted to −79.5 ppm and broadened to fwhm = 140 Hz. These NMR analyses revealed that the reduced phase contains a mixture (∼3:2 oxidized/reduced) of reduced and fully oxidized silicomolybdate clusters. However, powder X-ray diffraction confirmed that the two cluster types coexist in a single phase rather than two separate phases.

(36) Dolbecq, A.; Cadot, E.; Eisner, D.; Secheresse, F. *Inorg. Chem.* **1999**, *38*, 4217.
(37) Dec, S. F.; Herring, A. M. *J. Phys. Chem. B* **2004**, *108*, 12339.

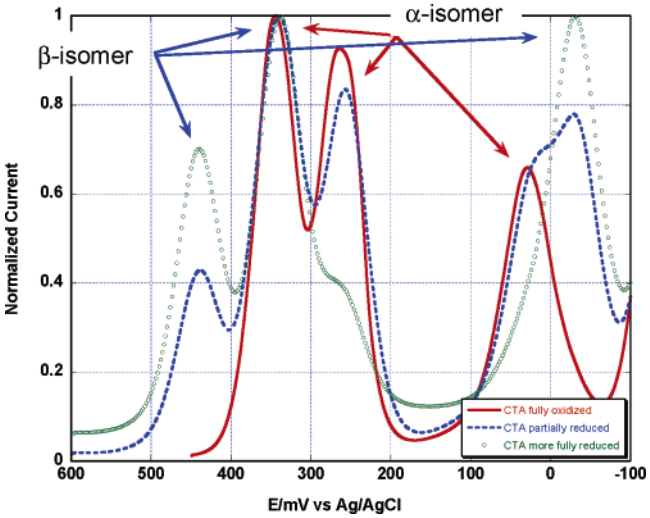

Figure 4. Overlay of the normalized difference Osteryoung square wave voltammetric response of $[SiMo_{12}][CTA]_4$ (fully oxidized) (red) and two reduced $[SiMo_{12}]$-CTA phases: 3-day MEK treatment (blue) and 7-day MEK treatment (green).

Electrochemical measurements proved useful not only for measuring the charge on each cluster type in the reduced phase but also revealed that the reduced cluster that corresponds with the −79.5 ppm ^{29}Si NMR chemical shift is in fact the β-Keggin cluster. The β-Keggin in the reduced phase is the two-electron reduction product with a −6 charge. The silicomolybdate anion exhibits a number of well-defined reversible multielectron redox reactions that can be used for speciation. As an example of this behavior, the cyclic voltammograms (CVs) of silicomolybdic acid and the fully oxidized (yellow) $[SiMo_{12}][CTA]_4$ phase over the potential range investigated show the first three redox processes that have each been previously identified as being two-electron reactions.[38,39] In the Osteryoung square wave voltammograms (OSWVs), both compounds exhibit essentially identical behavior. Furthermore, the open circuit potential of freshly prepared solutions of both of these compounds are also the same (450 mV). These data confirm that the electroactive species in the 1:4 phase is the α-Keggin ion.

In the case of the blue reduced phase (3-day treatment in MEK), the open circuit voltage of a freshly prepared solution is 445 mV, nearly the same as that of the fully oxidized yellow species. However, the CV data shows an oxidation wave on cycling to more positive potentials, which indicates that the compound is initially in a partially reduced form. Further inspection of the CV reveals a number of redox reactions in the range of 600 to −100 mV, some of which are found at the same potentials as those observed for the 1:4 phase. However, additional redox reactions can be attributed to those associated with the β-Keggin.[38,39] This is illustrated by comparison of the OSW voltammetric response as seen in Figure 4, where two new redox peaks are observed at 450 and −50 mV, and the original peak observed at 50 mV now appears as a shoulder on the larger peak at −50 mV. In the 7-day MEK treated sample, the current for the α-Keggin at 250 and 50 mV is reduced even further, and

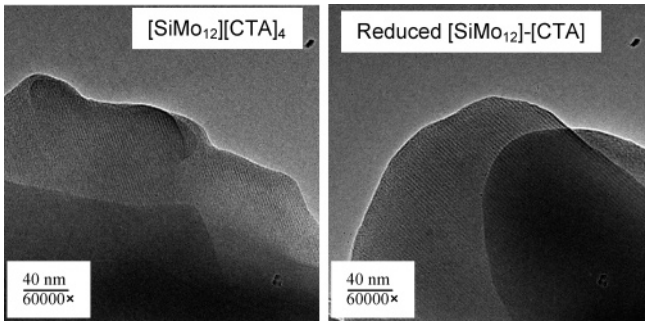

Figure 5. TEM images of $[SiMo_{12}][CTA]_4$ (left) and reduced $[SiMo_{12}]$-CTA (right). Both phases show a predominance of layered morphology. Basal spacing estimated by TEM: 25 Å for $[SiMo_{12}][CTA]_4$ and 33 Å for reduced $[SiMo_{12}]$-CTA.

the redox reactions associated with the β-Keggin now predominate. Finally, based on the relative peak areas of the different species present, particularly those centered at about 450 and 250 mV, the relative amounts of α- to β-Keggin are estimated to be in the range of approximately 3:2 in the 3-day MEK-reduced sample (confirming the ^{29}Si NMR result), with the α-Keggin being fully oxidized and the β-Keggin in the two-electron reduced form.

Specimens for powder X-ray diffraction analysis of the 1:4 phase and the reduced phase were prepared by evaporation of acetonitrile solutions on glass slides. This preparation technique increases the preferred orientation of the layers, which is necessary to better observe the diffraction peaks in the less-well ordered, reduced phase. The 1:4 phase shows very strong preferred orientation on the *ab*-face, and the basal (002) *d*-spacing is 22.7 Å. The single-crystal data lead to a layer spacing of around 20.5 Å. This discrepancy may be due to differences in the temperature of measurement (ambient temperature for X-ray powder analysis and 203 K for single-crystal analysis). Another explanation may be the inclusion of solvent molecules (i.e., water or acetonitrile) that slightly increases the *d*-spacing of the bulk of the 1:4 phase, whereas the single-crystal from which we obtained X-ray data contains no solvent molecules. The X-ray powder diffraction spectrum of the reduced $[SiMo_{12}]$ −CTA phase suggests less long-range order and less preferred orientation: the largest peak ($d = 34.0$ Å) is about 100× less intense than that of the 1:4 (002) peak. Furthermore, the fwhm of the basal peak for the 1:4 phase is 0.09°, and the fwhm of the first peak for the reduced phase is 0.39°. Transmission electron microscopy of the two silicomolybdate−CTA phases confirmed the morphology of layered materials, and both phases appear well-ordered at the length scale of TEM analyses. The basal layer *d*-spacings observed in the two phases by TEM (Figure 5) were estimated by counting the number of layers within 40 nm. These measurements were repeated throughout the sample for statistical averaging. This exercise showed that basal layering in both samples is uniform throughout the samples. The $[SiMo_{12}][CTA]_4$ phase has ∼16 layers in 40 nm, or 25 Å per layer. The reduced phase has ∼12 layers in 40 nm, or 33 Å per layer. These *d*-values agree reasonably well with those determined by X-ray powder diffraction.

Upon evaporation of acetonitrile solutions of $[SiMo_{12}]$-$[CTA]_4$ and reduced $[SiMo_{12}]$ −CTA, the precipitates that

(38) Massart, R.; Herve, G. *Rev. Chim. Miner.* **1968**, *L5*, 501.
(39) Souchay, P.; Massart, R.; Herve, G. *Rev. Polarogr.* **1967**, *14*, 270.

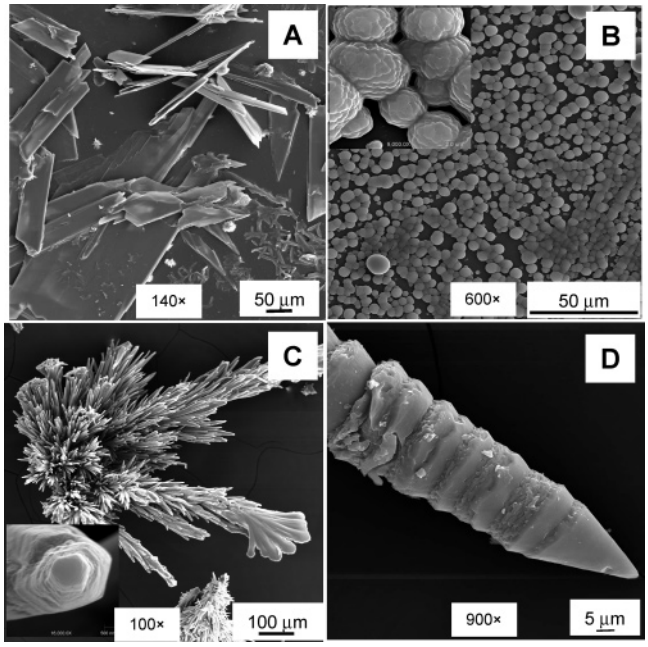

Figure 6. SEM images of $[SiMo_{12}][CTA]_4$ (A) and reduced $[SiMo_{12}]$-CTA (B−D) comparing the morphologies. (A) $[SiMo_{12}][CTA]_4$ from rapid evaporation of acetonitrile solution. (B) Reduced $[SiMo_{12}]$-CTA from rapid evaporation of acetonitrile solution. (C) Reduced $[SiMo_{12}]$-CTA from slow evaporation of acetonitrile. (D) Reduced $[SiMo_{12}]$-CTA from the MEK reduction solution.

remain are of very different morphologies. SEM images of both the 1:4 phase and the reduced phase are displayed in Figure 6. Panels A and B are $[SiMo_{12}][CTA]_4$ and reduced $[SiMo_{12}]$ −CTA, respectively, both grown by rapid evaporation of acetonitrile solutions (these are also the samples from which we obtain powder X-ray diffraction spectra). The 1:4 phase consists of lamellar crystals, which induces a very strong preferred orientation in the X-ray powder diffraction spectrum. Clearly, the preferred growth direction of the 1:4 phase is within the layers of anions and cations rather than perpendicular to the layers. The morphology of the reduced phase, on the other hand, suggests that the preferred growth direction is perpendicular to the layering, where the major stabilization interactions are cation−anion electrostatic interactions. Since this is the preferred growth direction in the reduced phase, it is likely that these are the strongest stabilization interactions in this phase. Several of the unusual morphologies of this phase can be seen in panels B−D. While panel B is from rapid evaporation of an acetonitrile solution, panel C is a very slow evaporation of acetonitrile, and panel D is from the MEK−water mixture in which the reduction took place. Close-up views of the both the precipitated spheres **(**panel B) and blades (panels C and D) show the presence of layers. In the case of the slow precipitation from acetonitrile (panel C), a hexagonal morphology is visible on the tip of the fingers.

Differential scanning calorimetry (DSC) (Figure 7) provided evidence for order and stability of the interdigitated surfactant tails in the 1:4 phase and relative disorder in the reduced phase. When heated, the 1:4 phase has three endothermic solid-state phase transitions in the region of 90−120 °C. These are correlated with increased disorder upon increasing the thermal energy of the surfactant tails.[7,40] With

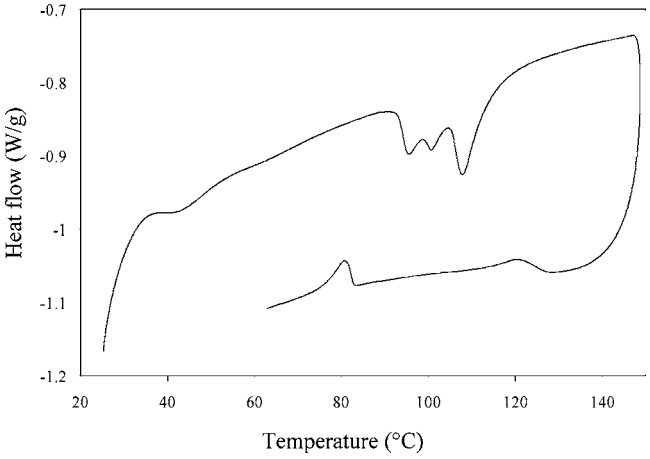

Figure 7. Differential scanning calorimetry of $[SiMo_{12}][CTA]_4$ showing solid-state phase transitions.

cooling, the DSC spectrum of the 1:4 phase shows an exothermic phase change at 80 °C, which likely corresponds with some reordering of the surfactant tails. The sample of $[SiMo_{12}][CTA]_4$ after the DSC experiment appears unchanged in color and shape. However, X-ray powder diffraction of the sample, postheating, reveals that the basal *d*-spacing is increased from ∼23 to ∼27 Å. This confirms that these endothermic and exothermic solid-state phase changes are indeed associated with alteration of surfactant tail interdigitation or tilt-angle. The reduced phase, on the other hand, shows no evidence for any solid-state phase transitions, which implies the surfactants tails are already relatively disordered at room temperature. The fact that there are anion clusters with either a −4 or −6 charge and slightly different geometries (α- or *β*-Keggin) in a single phase likely creates more disorder of the inorganic layers, in that attractive and repulsive forces along the interface of the cations and anions vary with some irregularity.

Finally, on the basis of the previous discussion, we attribute the preferred growth within the *xy*-plane of the 1:4 phase to the stability achieved by nearly complete interdigitation of the surfactant chains. The interdigitation provides energetic stability by increasing hydrophobic−hydrophobic interactions, decreasing hydrophobic−hydrophilic interactions, and increasing entropy by solvent exclusion.[40,41] The reduced phase does not appear to be so strongly interdigitated (by its larger layer *d*-spacing), is likely to be more disordered, and, therefore, probably does not achieve the equivalent stability by growth in the plane parallel to the layer direction.

Characterization of Additional POM−CTA Phases. The POM−CTA phases with POM charges ranging from −3 to −16 are all insoluble in water, due to their hydrophobic nature. The lower charged POM phases (i.e., $[PW_{12}O_{40}][CTA]_3$ and $[SiMo_{12}O_{40}][CTA]_4$) are soluble in acetone, acetonitrile, and methyl ethyl ketone and insoluble in alcohols. The intermediate charged POM phases ($[HNb_6O_{19}][CTA]_7$ and $[Ti_2Nb_8O_{28}][CTA]_8$) are soluble in short chain alcohols such as ethanol, *n*-propanol, and isopropanol. The higher-charged POM phases ($[H_2Si_4Nb_{16}O_{56}][CTA]_{14}$ and

(40) Landi, E.; Vacatello, M. *Thermochim. Acta* **1975**, *12*, 141.
(41) Gross, A. F.; Yang, S.; Navrotsky, A.; Tolbert, S. H. *J. Phys. Chem. B* **2003**, *107*, 2709.

Table 2. Comparison of Structural Features of 1:4 Surfactant Tail/Cluster Phases

	structural feature						
phase	anion charge	tails per surfactant	anion and cation arrangement	av cluster to cluster distance (Å)	% distortion[a] 100 (max−min)/av	tail interdigita tion	bilayer tilting
$[SiMo_{12}][CTA]_4$	4	1	hexagonal	12.40	9.8	yes	yes
$[Sn_2S_6][C_{12}H_{25}NH_3]_4 \cdot 2H_2O$[21]	4	1	distorted	9.68	27.2	yes	no
$[Ge_4S_{10}][CnH_{2n+1}NH_3]_4$ ($n = 12-18$)[8]	4	1	hexagonal	9.40 ($n = 14$) 9.34 ($n = 12$)	15.2 ($n = 14$) 10.4 ($n = 12$)	yes	no
$[Ge_4S_{10}][C_nH_{2n+1}N(CH_3)_3]_4$ ($n = 12, 14, 16, 18$)[7]	4	1	hexagonal	10.63 ($n = 12$) 10.66 ($n = 18$)	5.7 ($n = 12$) 6.1 ($n = 18$)	yes	yes
$[Ge_4Se_{10}][C_nH_{2n+1}N(CH_3)_3]_4$ ($n = 8,9$)[9]	4	1	hexagonal	11.09 ($n = 9$)	5.2	yes	yes
$[H_2V_{10}O_{28}][C_{12}H_{25}N(CH_3)_3]_4$[23,24]	4	1	distorted	11.72	32.3	yes	yes
$[Cr_2O_7][(C_{16}H_{33})_2(CH_3)_2N]_2$[22]	2	2	distorted	8.12	25.3	no	yes
$[Mo_6O_{19}][(C_{18}H_{36})_2N(CH_3)_2]_2$[25]	2	2	distorted	9.62	35.1	no	yes

[a] min, max, av = respectively, minimum, maximum, and average of six next nearest neighbor cluster-to-cluster distances.

$[SiNb_{12}O_{40}][CTA]_{16}$) are soluble in more hydrophobic alcohols such as pentanol and butanol. In other words, the higher the charge of the cluster, the more surfactant molecules and the more hydrophobic the cluster-surfactant phase. All of the POM−CTA phases appear to be approximately lamellar by powder X-ray diffraction in that the first two basal layer peaks are observed. Additionally, TEM studies revealed layers as the dominant morphological feature. By powder X-ray diffraction, all phases showed more preferred orientation and order when deposited by slow solution evaporation rather than precipitated instantaneously out of aqueous solution during the synthesis of the bulk powder.

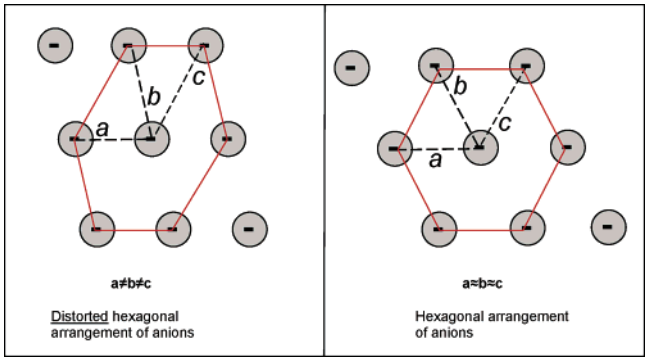

Figure 8. Cartoon illustrating a distorted hexagonal (left) and hexagonal (right) arrangement of a single layer of cluster anions of reported 1:4 cluster/surfactant phases.[7−9,21−25]

Discussion

This section includes: (1) a comparison of the general structural features of $[SiMo_{12}][CTA]_4$ to those of other reported 1:4 phases, (2) a discussion and comparison of the additional POM−CTA phases, (3) a comparison of parent surfactant salts to the cluster−surfactant phases, and (4) a brief discussion of the POM−TTF phases, another hybrid organic−inorganic system related to the cluster surfactant phases. Structural and chemical features that may influence or inhibit these phases to crystallize are highlighted in the following discussions.

Comparison of 1:4 Cluster−Surfactant Phases. To better understand the apparent uniqueness of the 1:4 ratio, we have summarized in Table 2 the general structural features of cation−anion arrangements of $[SiMo_{12}][CTA]_4$ and the other reported[7−9,21−25] 1:4 phases. The general structural features of $[SiMo_{12}][CTA]_4$ include (1) approximate hexagonal arrangement of the clusters and surfactants within the *xy*-plane, (2) sandwiching of the anionic layer between two cationic layers, (3) deep interdigitation of the surfactant tails, and (4) tilting of the surfactant tails. The sandwiching of the anion layer between two cation layers is the only of these structural features shared by all the 1:4 phases summarized in Table 2. There is some variability in the other characteristics. All of the 1:4 phases have a cation−anion arrangement that varies from hexagonal to distorted hexagonal, and these are illustrated in the cartoon in Figure 8 for an anion layer. In the case of extreme distortion, the arrangement approaches that of a square grid. In a hexagonal arrangement, $a \approx b \approx c$, whereas in the distorted hexagonal arrangement, $a \neq b \neq c$. Listed in Table 2 is the average cluster−cluster distance in the hexagonal or distorted hexagonal array (average of *a*, *b*, and *c* shown in Figure 8). Also shown is the % distortion (see Table 2), which is a term we use to describe the degree of distortion of the hexagonal array. Increasing the distortion of the hexagonal array is correlated with an increase in value of this term, where the most distorted (phase featuring Mo_6O_{19}) approaches a square grid arrangement. In general, it is observed that surfactant−cluster phases hosting clusters with more spherical shapes (such as Ge_4E_{10} or $SiMo_{12}O_{40}$) adopt the less distorted hexagonal geometry and that phases with clusters of a more anisotropic shape (i.e., Sn_2S_6, Cr_2O_7, $H_2V_{10}O_{28}$) adopt the distorted arrangement. The exception is the Mo_6O_{19} cluster, but this phase features the two-tail surfactant, which likely has a strong influence on the overall cluster−surfactant phase geometry. An increase in the average cluster−cluster distance of a phase correlates with increased cluster size, increased cationic head size, and slightly with increased surfactant tail length.

We also compared the area of the cluster anion to that of the surfactant cation head at the interface between the cation and the anion layers. These areas were compared by weighing a cutout of a space-filling model (Diamond 2.0) for the cation and anion, respectively, projected on the basal plane for each phase. The anion area:cation area ratio calculated by this method ranged from 1.8 to 4.3 for the various 1:4 phases, with no distinct trends observed.

Comparison of 1:4 Phases to Cluster−Surfactant Phases of Different Ratios. All the POM−surfactant phases synthesized in this study and discussed next were characterized by TEM and X-ray powder diffraction. These charac-

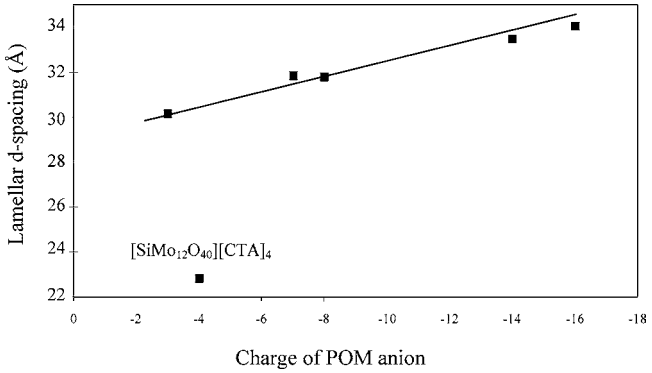

Figure 9. Plot of layer *d*-spacing (Å) of the POM-CTA phases as a function of POM anion charge.

terizations showed that the prominent morphological and structural feature of these phases is strong layering with spacing between 20 and 35 Å. Figure 9 shows a plot of the basal *d*-spacing (Å) of the POM−CTA phases as a function of POM anion charge. There is a linear correlation (R^2 = 98%) between the anionic cluster charge and the basal layer *d*-spacing for all the phases except for $[SiMo_{12}O_{40}][CTA]_4$, which has significantly smaller *d*-spacing relative to the linear trend. The report by Stein et al. also noted a linear increase in *d*-spacing with an increase in cluster charge from −4 to −5 to −6, which they attributed to needing more space to pack additional surfactant cations.[26] These data reinforce the supposition that the 1:4 ratio is unique in terms of structure ordering. In the structure of $[SiMo_{12}O_{40}][CTA]_4$, it is noted that the C_{16} tails are almost completely interdigitated and that they are tilted from the normal to the plane of the $[SiMo_{12}O_{40}]^{4-}$ anions. Both geometric accommodations, especially the tail interdigitation, result in a decrease in the layer spacing in the direction normal to the alternating anion layers and lipid bilayers. We can understand why the layer spacing of a POM−CTA phase must expand if more surfactant heads are packed around the anionic clusters by making some assumptions on the best location for additional cation heads, based on minimizing cation−cation repulsions and maximizing cation−anion interactions. Upon viewing the charged layers of the 1:4 structure in Figure 2, one might imagine the next logical place to put an ammonium head in this already-compact hexagonal array of cations and anions is directly above or below the cluster, located at the center of the cluster when viewed down the *c*-axis. This cation placement also hypothetically transitions the structure a step closer to that of the surfactant-encapsulated (SEC) motif of the higher-charged clusters, in which the surfactant heads completely enclose the cluster.[15,16,19] By this placement of cation heads, the corresponding tails are offset from the surfactant tails whose heads are interpenetrating with the anion layer. Therefore, these additional surfactant cations actually would not fit between the anion cluster layers of the 1:4 phase, as illustrated in the cartoon in Figure 10. This insertion of extra surfactants can thus be accommodated by moving the anionic layers apart (increasing the *d*-spacing), decreasing the interdigitation of the surfactant tails, and thus decreasing the overall stability.

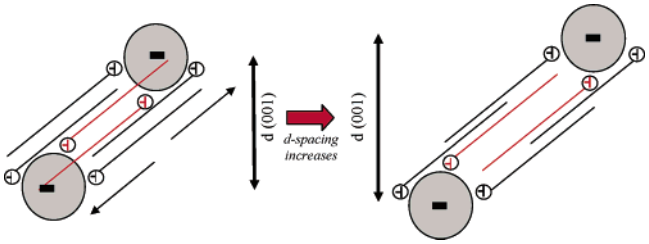

Figure 10. Cartoon illustrating how *d*-spacing might increase with increasing POM charge in POM-CTA phases. The gray circles represent the anionic POMs. The black surfactant molecules are present in the 1:4 phase. The red surfactant molecules are placed to maximize cation−anion interaction and minimize cation−cation interaction in a phase with the POM charge beyond −4 (see text).

Comparison of Cluster−Surfactant Phases to Parent Surfactant Salts. The structures of parent surfactants such as CTABr are also relevant to this current discussion. A number of surfactant cations charge balanced by simple, monomeric anions have been characterized by single-crystal X-ray diffraction (see Abdallah et al.[42] and Kunitake[35] and references therein). Generally, all the single-tail surfactants are interdigitated in lipid bilayers, whereas the double-tail surfactants are not interdigitated and have one straight tail and one bent tail that was described in the cluster−surfactant phases[22,25] featuring two-tail surfactants. Additionally, tilting of the chains is common for both single- and double-chain phases. Presumably, these conformations are adopted to match the space-filling requirements of both the hydrophilic and the hydrophobic sections of the surfactant molecules.[35] In fact, the two cluster−surfactant phases that do not exhibit chain tilting contain the ammonium surfactant, whereas the other structures that do have tilted tails feature the trimethylammonium surfactant (see Table 2). The trimethylammonium head necessarily requires more space than the ammonium head. Thus, the tails of the trimethylammonium surfactants tilt to match the cross-sectional space-filling area of the tail to the head, whereas the cross-sectional areas of the ammonium head and tail match without tail tilting. Much of this evidence suggests that these structural features observed in the various cluster−surfactant phases are essentially controlled by the surfactant assembly rather than the cluster assembly. Furthermore, this implies that anions of −1, −2, and −4 charge best match the template created by a surfactant assembly since these are the anion charges of all surfactant salts studied by single-crystal diffraction (to our knowledge). Apparently, the phases featuring anions with >-4 charge necessarily have buckled and distorted layers to assemble a larger number of cationic species around these clusters of more negative charge. This in turn does not allow for order and deep interdigitation of the surfactant tails and results in increased lamellar *d*-spacing. Finally, we address the issue of phases featuring anions with a −3 charge, such as $[PW_{12}O_{40}][CTA]_3$. It is noted that this 1:3 cluster−surfactant phase also has a much larger *d*-spacing (∼30 Å) than the 1:4 phase, and it has the poorest long-range ordering of all the phases we have investigated, as observed by its weak and broad powder X-ray diffraction reflections. Dis-

(42) Abdallah, D. J.; Bachman, R. E.; Perlstein, J.; Weiss, R. G. *J. Phys. Chem. B* **1999**, *103*, 9269.

order is observed in this phase probably because good packing of the inorganic layer with the lipid bilayer array cannot be achieved by a 1:3 cluster:surfactant ratio.

POM−Organic Donor Phases. Finally, it is worth mentioning in this discussion the hybrid compounds formed by POM and organic donors of the TTF-type (TTF = tetrathiafulvalene, BEDT-TTF = bis(ethylenedithio)TTF), which are charge-transfer salts that possess interesting conduction and magnetic properties.[5,43] Like the cluster−surfactant phases, most of them assemble as POM layers alternating with layers of cationic, organic molecules. One important difference between the surfactant molecules and the organic donors is the tendency of the donors to form one- and two-dimensional packings, due to the orbital overlap between the sulfur atoms. These organic ligands are relatively short and rigid as compared to the surfactant molecules: the TTF cation can be described as ∼6 atoms along its long dimension (two linked rings), and the BEST and BEDT cations are approximately 10 atoms long (four linked rings). Another difference is the possibility of these molecules to be present in the solid as neutral or charged molecules (with charges ranging from +2 to <+1). Given all these variables, one would expect greater flexibility for crystallizing phases featuring POMs of >−4 charge, as seems to be the case. Comparable to the cluster−surfactant phases, crystal structures of TTF−organic donor compounds have been mostly reported for POM clusters possessing negative charges ≤4. These POM clusters include $[Mo_8O_{26}]^{4-}$,[44] $[M_6O_{19}]^{2-}$ (M = Mo,W),[45] and $[XM_{12}O_{40}]^{4-}$ (X = Si, P; M = Mo, W).[46] In most of these compounds TTF molecules are forming chain structures or surrounding the POMs. With the BEDT-TTF (bis(ethylenedithio)TTF) and its derivatives BEST (bis-(ethylene-diseleno)-tetraselenofulvalene) and BEDO-TTF (bis(ethylenedithio)-tetraoxofulvalene), the tendency of these cations to form two-dimensional structures dominates. Thus, structures formed by alternating layers of cations and anions are obtained. It is to be noted that most of the polyanions having the Keggin structure share a charge of −4. This tendency is seen, for example, in the $[PMo_{12}O_{40}]^{3-}$,[47] which is reduced by one electron to afford the tetraanion, or in the highly charged substituted anions $[XW_{12}O_{40}]^{n-}$ (X = Co(II), Cu(II), Fe(III), B(III)), which tend to be protonated to reduce their negative charge.[48] With other POMs, layered materials are also obtained for charges comprised between −2 and −6. These POMs include $[H_3V_{10}O_{28}]^{3-}$,[49] $[VW_5O_{19}]^{3-}$,[50] and $[P_2W_{18}O_{62}]^{6-}$.[51] There are also reports of salts containing anions with higher charges, such as $[Co_4(H_2O)_2(PW_9O_{34})_2]^{10-}$,[52] but no crystal structures are reported.

Conclusions

The experimental studies and comparative literature reviews presented in this paper have suggested that there are numerous factors that influence the ability to form well-ordered phases of cluster anions and cationic surfactant lipid bilayers. The unique features of the 1:4 phases containing single-tail surfactants include deep interdigitation of the surfactant tails and hexagonal or distorted hexagonal arrangement of both cations and anions for optimal packing and electrostatic interactions. The phases containing double-tail surfactants display distorted-hexagonal ordering of cations and anions, no interdigitation of the surfactant tails, and one straight plus one bent tail per surfactant molecule. These features of phases containing single- and double-tail surfactants also hold true for the parent surfactant salts, which suggests that the order of the surfactant ions has the biggest influence on the structure of the corresponding cluster−surfactant phases. However, the geometry of the cluster appears to influence the distortion of the hexagonal array of cations and anions.

The study on the MEK-reduced $[SiMo_{12}]$ −CTA phase brought to light a number of other factors that might impact the formation of well-ordered lipid bilayers and anion layers. In particular, these features include the incorporation of solvent molecules or small charged-species (i.e., H_2O or H_3O^+) in either the hydrophilic or the hydrophobic regions of the phase and variability in clusters charge and/or structure. The investigations of POM−CTA phases with a range of POM charges from −3 to −16 showed that the dominant morphology of all these phases is layers that have *d*-spacings ranging from ∼20 to 35 Å and increase as a function of POM charge. While single-crystal studies provide exact structural information about the 1:4 phases and techniques such as small angle scattering have been used to define the structure of the surfactant-enclosed clusters of charges >−20, the structures of the phases in the intermediate cluster charge ranging between −4 and −20 continue to elude us. However, by using simple space-filling and electrostatic arguments, we presented here suggestions of how the structure of cluster−surfactant phases could evolve from flat layers to distorted layers and how this could result in an increase in *d*-spacing while maintaining a predominantly lamellar morphology. We believe computational studies and use of advanced X-ray diffraction techniques (i.e., synchrotron) for analyzing smaller and poorer quality crystals will provide more detailed models of these phases soon. Therefore, we will continue these investigations by attempting crystal growth of a variety of phases including both the proven 1:4 cluster-to-surfactant ratio, as well as the more challenging phases containing higher charge clusters and larger surfactant:cluster ratios.

(43) Ouahab, L. *Coord. Chem. Rev.* **1998**, *178−180*, 1501.
(44) Gomez-Garcia, C. J.; Coronado, E. *Synth. Met.* **1993**, *55−57*, 1787.
(45) Triki, S.; Ouahab, L.; Halet, J.-F.; Pena, O.; Padiou, J.; Grandjean, D.; Garrigou-Lagrange, C.; Delhaes, P. *J. Chem. Soc., Dalton Trans.* **1992**, 1217.
(46) Ouahab, L.; Bencharif, M.; Mhanni, A.; Pelloquin, D.; Halet, J.-F.; Pena, O.; Padiou, J.; Grandjean, D. *Chem. Mater.* **1992**, *4*, 666.
(47) Coronado, E.; Galan-Mascaros, J. R.; Gimenez-Saiz, C.; Gomez-Garcia, C. J.; Falvello, L. R.; Delhaes, P. *Inorg. Chem.* **1998**, *37*, 2183.
(48) Gomez-Garcia, C. J.; Gimenez-Saiz, C.; Triki, S.; Coronado, E.; Le Magueres, P.; Ouahab, L.; Ducasse, L.; Sourisseau, C.; Delhaes, P. *Inorg. Chem.* **1995**, *34*, 4139.
(49) Coronado, E.; Galan-Mascaros, J. R.; Gimenez-Saiz, C.; Gomez-Garcia, C. J.; Martinez-Ferrero, E.; Almeida, M.; Lopes, E. B. *Adv. Mater.* **2004**, *16*, 324.
(50) Ouahab, L.; Golhen, S.; Triki, S.; Lapinski, A.; Golub, M.; Swietlik, R. *J. Cluster Sci.* **2002**, *13*, 267.
(51) Coronado, E.; Galan-Mascaros, J. R.; Gimenez-Saiz, C.; Gomez-Garcia, C. J.; Laukhin, V. N. *Adv. Mater.* **1996**, *8*, 801.
(52) Gomez-Garcia, C. J.; Borrass-Almenar, J. J.; Coronado, E.; Delhaes, P.; Garrigou-Lagrange, C.; Baker, L. C. W. *Synth. Met.* **1993**, *55−57*, 2023.

Acknowledgment. The authors thank the Sandia LDRD program for funding for this work. Sandia is a multiprogram laboratory operated by the Sandia Corporation, a Lockheed Martin Company, for the United States Department of Energy under Contract DE-AC04-94AL85000. We thank Prof. Eugenio Coronado for helpful discussions.

Supporting Information Available: Crystallographic CIF file for $[SiMo_{12}O_{40}][CTA]_4$, IR spectra for $[SiMo_{12}O_{40}][CTA]_4$ and the reduced phase, and powder X-ray diffraction spectra of $[SiMo_{12}O_{40}][CTA]_4$ and the reduced phase. This material is available free of charge via the Internet at http://pubs.acs.org.

CM0503174